JOURNAL OF EARTH SCIENCES AND TECHNOLOGY

www.journals.procedia.org/

Journal of Earth Sciences and Technology (1)1 2019 1–15

Mapping the Concentrations of Total Suspended Sediment Using ALOS Data in Coastal Waters of Langkawi Island, Malaysia

M. Moussavi Alashloo[a]*, S.Y. Moussavi Alashloo[b], Lim Hwee San[a],

[a]*School of Physics, Universiti Sains Malaysia, 11800 Penang, Malaysia*
[b]Department of Geosciences, Universiti Teknologi PETRONAS, 32610 Seri Iskandar, Perak Malaysia

Abstract

Remote sensing method is a powerful tool for water quality monitoring and modeling via analyzing satellite images of a widespread area. This study presents the development of regression models for estimating and mapping concentrations of total suspended sediment (TSS) over the coastal waters of Langkawi Island, Malaysia from Advanced Land Observation Satellite (ALOS) images. Two ALOS images and nearly contemporaneous in situ measurements of TSS were utilized. The digital numbers for each visible band corresponds to the sea-truth positions were identified and were transformed into reflectance values. The relationships were investigated between TSS concentrations and reflectance of ALOS bands. The non-linear relationship between in-situ TSS and reflectance combinations of the three visible bands demonstrated the highest correlation with a low root-mean-square error (RMSE $\approx$ 3.52mg/l) and high correlation coefficient (R2 = 0.91). The results confirm that the proposed algorithm obtained from ALOS data is successful for TSS mapping of the coastal waters of Langkawi Island, Malaysia.

Keywords: ALOS imagery; Remote sensing; Langkawi Island; TSS; Suspended sediment

1. Introduction

Water pollution problem becomes increasingly critical nowadays. Water, as one of the most precious natural resources, serves as the lifeblood that sustains development in any society. With decrease in water resources, it is essential to protect water resource and properly manage environmental activities to sustain the quality of life on earth. The condition of surface water in the estuary of streams, reservoirs, lakes, and oceans is a key environmental indicator that illustrates the overall health of the coastal ecosystem. According to Guan et al. (2011), concentration of suspended sediment, which causes non-point source pollution, is one of the most significant water quality parameters in coastal waters. Suspended substances, used as carriers to store the agents of pesticides to absorb nitrogen, phosphorus, and organic materials, can be indicators on levels of pollution (Park & Latrubesse, 2014; W. Zhou et al., 2006). Therefore, controlling and assessing the concentration of suspended material in coastal waters is crucial.

* Corresponding author. Tel.: +60174391603
E-mail address: maryamalashloo@gmail.com

Zhou et al. (2006) demonstrated that it is difficult to obtain synoptic information on water quality from a routine in-situ monitoring network. In coastal waters, typical measurements of water quality require in-situ sampling as well as time-consuming and expensive laboratory effort (Bresciani et al., 2012; Matarrese et al., 2011). Furthermore, conventional measurements are not enough to highlight regional and global water quality issues and address water quality distribution patterns in bodies of water (Asadpour et al., 2011; H. Lim et al., 2010). Hence, the hardship of successive and synoptic water quality sampling is an obstacle to water quality monitoring, forecasting, and management (Shafique et al., 2001).

Remote sensing is an appropriate approach to conduct an effective water resources monitoring program (Bresciani et al., 2012). Remote sensing has been used broadly for water studies and has played an influential role in environmental management strategies and water quality assessment. Trends in the coastal environment can be evaluated through remotely-sensed TSS without the need of sampling in situ. Several investigations have been executed on the effectiveness of remotely sensed data to solve the deficiency of conventional techniques (Kabbara et al., 2008; H. Lim et al., 2011; Long & Pavelsky, 2013; Massi et al., 2011; Matarrese et al., 2011; Nagamani et al., 2012; Randolph et al., 2008; Zawada et al., 2007). Since the 1970s, data from satellites have been employed for remote sensing studies of suspended sediments (Hellweger et al., 2004). Satellite imagery has been extensively utilized for coastal water quality inspections (Kabbara et al., 2008; Matarrese et al., 2011).

The relationship between concentrations of water quality parameters and satellite data has been studied for several decades (Bresciani et al., 2012; Matarrese et al., 2011), and various model-based estimation algorithms have been produced. Two different methods namely inversion of semi-analytical modeling, and empirical analysis helped to create these algorithms (Giardino et al., 2007). Analytical models involve inverting four relationships to find out water quality parameters from the remote sensed data, in accordance with the order of the water quality parameters, the bulk Inherent Optical Properties, the specific Inherent Optical Properties, the Top of Atmosphere radiance and the Apparent Optical Properties. In empirical techniques, regression approaches are widely used and the algorithms were established in reliance on the water reflectance model, a function of the inherent optical properties of water. This approach is based on developing multivariate regressions between the ground measurement water quality parameters and the remotely sensed reflectance data. Therefore, to correlate water quality with remote sensing measurements, different models have been developed. The regression analysis of satellite data and simultaneous measurements of ground observation data has been the common practice in remote sensing of coastal waters. Previous researches have presented that reliable empirical relationships can be created between ground observations of suspended sediments and satellite (Abdullah et al., 2002; Bruzzone & Melgani, 2005; Hariyanto et al., 2011; H. Lim et al., 2011). Hakvoort et al. (2002) used regression models that do not need any complementary ground data. They applied a matrix inversion technique, required specific inherent optical properties, and reflectance spectra to calculate concentrations of water components. In this research, a multispectral regression algorithm is derived from water reflectance model, which is related to the inherent optical properties of water. These features can then be connected to the concentration of total suspended sediment (TSS).

The objective of this study is to explore the application of the recently proposed algorithm for determining the TSS concentration that is conducted using high resolution ALOS imagery and in-situ data of the coastal waters of Langkawi Island. The algorithm, developed in this study, has been determined from the reflectance model for TSS. Eventually, the algorithm was applied to create the distribution TSS concentration maps.

2. Study area

In this study, the southern, western and northwestern coastal waters of Langkawi Island are investigated. Langkawi Island, is located in the northwest coast of Peninsular Malaysia, close to the border of Thailand and is located approximately at latitude 6° 5’N to 6° 35’N and longitude 99° 35’E to 99° 55’E (Figure 1). The island has an area of 362 km2 and it has become an attractive destination for both domestic and international tourists in recent years. Nevertheless, agriculture and industry are

reported to be the leading potential source of island's water pollution (Jordao et al., 2002). The estuarine and coastal areas of Langkawi Island are the locations where a great amount of sediment is entered into the ocean system via terrestrial runoffs, rivers, and leachates carrying chemicals originated from numerous urban areas. This is because of the quick growth of the district through development of the industrialization zone along with the raise in population. Commercial organizations such as resorts, hotels, shopping malls, marine recreational facilities, and jetties have been advanced along the island's shoreline to support the increasing number of visitors. This huge development instantly influences marine ecosystem productivity and leads to contamination in the seaside and neighboring areas (Kamaruzzaman et al., 2010).

Fig. 1. The location of study area in the northwest coast of Peninsular Malaysia (adapted from Google Earth).

3. Methodology

3.1 Satellite data

An ALOS Advanced Visible and Near Infrared Radiometer type 2 (AVNIR-2) tool was employed as the imaging sensor system to measure TSS concentration in the coastal waters of Langkawi Island, as shown in the study area. The satellite images were acquired on 13.01.2008 and 18.01.2010. The ALOS was become operational on 26 January 2006. The ALOS possesses two optical sensors: Panchromatic Remote-sensing Instrument for Stereo Mapping (PRISM) for digital elevation mapping and AVNIR-2 for accurate land coverage monitoring. The AVNIR-2 is a visible and near infrared radiometer that is utilized to observe regional environments, such as coastal zones, water bodies, and lands. AVNIR-2 was introduced after AVNIR, which was on board the Advanced Earth Observing Satellite launched in August 1996. The instantaneous field-of-view is the principal enhancement of AVNIR-2 over AVNIR. Furthermore, AVNIR-2 supplies 10 m of spatial resolution images, an upgrade over the 16-m resolution of AVNIR in the multi-spectral region (H. S. Lim et al., 2013). The details of ALOS are expressed in table 1, and the raw ALOS AVNIR-2 satellite scene is illustrated in figure 2.

Table 1. Details of ALOS, AVNIR-2 utilized in this research (H. Lim et al., 2009)

General Features	Details	
Launch date	26 January 2006	
Launch site	Tanegashima Space Centre, Japan	
Design life	3-5 years	
Repeat cycle	46 days	
Altitude	691.65 km	
Number of bands	4	
Wavelength	Band 1 (Blue)	420-500 nm
	Band 2 (Green)	520-600 nm
	Band 3 (Red)	610-690 nm
	Band 4 (Near Infrared)	760-890 nm
Swath width	70 km	
Spatial resolution	10 m	

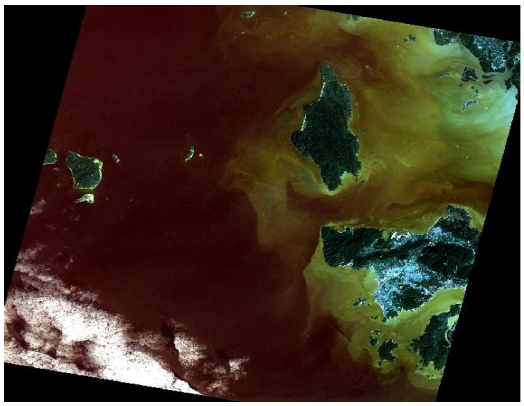

Fig. 2. Raw satellite image.

3.2 In-Situ data collection

The simultaneous complementary in-situ water samples were acquired from a boat as the ALOS passed over the study area. The collected samples were stored in polyethylene bottles. The sampling locations were cautiously chosen to include a wide range of TSS concentrations and to be representative of the study areas. The water samples were filtered through 0.45 μm nuclepore ultracellulose membrane filters and analyzed to calculate the TSS concentrations. The standard method developed by Strickland and Parsons (1972) is used to carry out the analysis. A handheld global positioning system (GPS) is used to determine the sampling locations. The water sampling points are indicated in figure 3. The locations and statistical results of the calculated value of TSS from collected water samples of the coastal waters of Langkawi Island on 13.01.2008 and 18.01.2010 are shown in table 2. The measured TSS concentrations ranged from 70 mg/l to 120 mg/l.

3.3 Optical model of water

Remote sensing reflectance plays an important role in optical water studies (Asadpour et al., 2012; Syahreza, Jafri, et al., 2011). Water-quality surveys based on remotely sensed data are normally centred on computing the radiance from the water column and the concentrations of water quality exiting toward the sensor. The reflected energy emitted by water bodies is especially dependent on the inherent optical properties of water such as the backscattering coefficient and the absorption coefficient.
Remote sensing reflectance, R_{rs} unitless, is related to the irradiance reflectance just beneath the water surface, R_{ird} (Doxaran et al., 2002), and is measured as:

$$R_{ird} = \frac{(1-\rho)(1-\sigma)R_{rs}}{n^2(1-xR_{rs}R)Q} \quad (1)$$

where σ = air-water Fresnel reflection at the interface
ρ = internal Fresnel reflectance
n = refractive index (1.34)
x = water-air reflection.

Q is the upwelling irradiance to upwelling radiance ratio (in sr), which would be π if the upwelling radiance distribution were isotropic, but may vary between approximately 3.1 and 5.6 (Doxaran et al., 2002). According to Doxaran et al. (2002), equation (1) can be approximated as:

$$R_{rs} = 0.182\,\frac{R_{ird}}{Q} \quad (2)$$

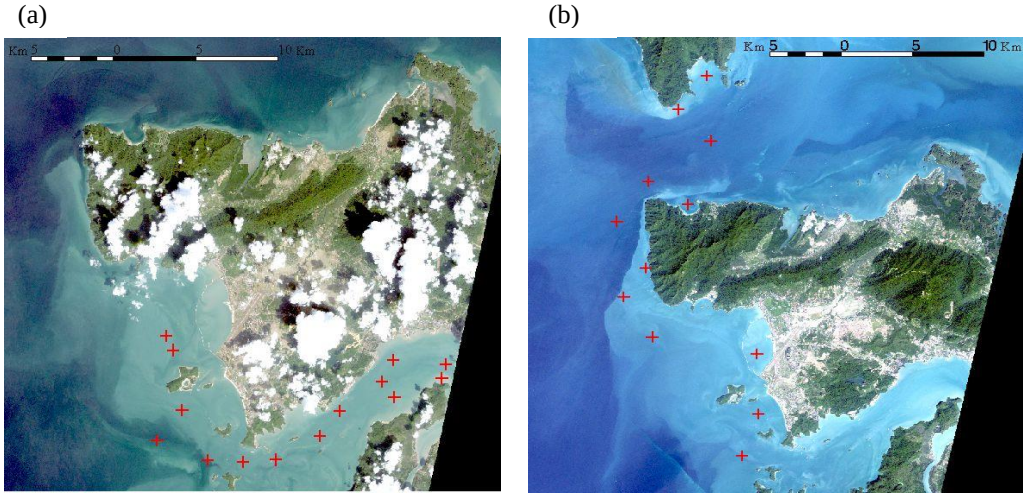

Fig. 3. Location of sampling stations in the Langkawi Island coastal waters on (a) 13.01.2008; (b) 18.1.2010.

Table 2. Location of sampling sites and measured TSS concentrations on (a) 13.01.2008; (b) 18.01.2010.

(*a*)

Site	longitude	latitude	TSS *(mg/l)*	Site	longitude	latitude	TSS *(mg/l)*
1	99˚41'9.23" E	6˚19'14.77" N	95	8	99˚46'12.26" E	6˚15'55.05" N	79
2	99˚41'22.21" E	6˚18'46.09" N	90	9	99˚46'52.69" E	6˚16'44.49" N	86
3	99˚41'40.27" E	6˚16'46.23" N	81	10	99˚48'16.09" E	6˚17'42.98" N	85
4	99˚40'50.73" E	6˚15'47.68" N	75	11	99˚48'38.29" E	6˚18'25.93" N	91
5	99˚42'30.91" E	6˚15'7.17" N	72	12	99˚48'40.78" E	6˚17'11.68" N	98
6	99˚43'41.2" E	6˚15'4.47" N	85	13	99˚50'14.56" E	6˚17'49.3" N	119
7	994˚4'44.98" E	6˚15'8.29" N	78	14	99˚50'22.41" E	61˚8'16.64" N	102

(*b*)

Site	longitude	latitude	TSS	Site	longitude	latitude	TSS *(mg/l)*
1	99˚40'48.21" E	6˚31'31.47" N	89	7	99˚38'27.63" E	6˚23'13.99" N	88
2	99˚39'42.78" E	6˚30'4.47" N	105	8	99˚37'37.8" E	6˚21'59.4" N	90
3	99˚40'57.31" E	6˚28'43.5" N	78	9	99˚38'42.96" E	6˚20'16.68" N	85
4	99˚38'34.31" E	6˚28'57.9" N	72	10	99˚42'42.28" E	6˚19'32.83" N	112
5	99˚40'4.23" E	6˚25'58.72" N	82	11	99˚42'45.17" E	6˚16'57.3" N	109
6	99˚37'22.49" E	6˚25'15.38" N	76	12	99˚42'7.73" E	6˚15'8.49" N	87

The irradiance reflectance $R_{ird}(\lambda)$ just below the water surface is (Kratzer et al., 2008; Siddorn et al., 2001):

$$R_{ird}(\lambda) = 0.33\frac{b_w(\lambda)}{a(\lambda)} \tag{3}$$

where λ represents the spectral wavelength, b_w denotes the backscattering coefficient, and *a* refers to the absorption coefficient. The method to derive the equation 3 is described in detail in our prior article (H. Lim et al., 2010). The inherent optical properties of water are determined by the water content. The contributions of the individual components to the overall properties are strictly additive (Gallegos & Correll, 1990). In a case including three water-quality components, namely, suspended sediment P, yellow substance Y, and chlorophyll C, the simultaneous equations for the three channels (λ_1, λ_2, and λ_3) can be demonstrated as (H. Lim et al., 2010):

$$R_{rs}(\lambda_1) = R_1 = \frac{c}{Q}\frac{[0.5b_{bw}(\lambda_1)+b_c^*(\lambda_1)C+b_p^*(\lambda_1)P]}{[a_w(\lambda_1)+a_c^*(\lambda_1)C+a_p^*(\lambda_1)P+a_y^*(\lambda_1)Y]} \tag{4}$$

$$R_{rs}(\lambda_2) = R_2 = \frac{c}{Q}\frac{[0.5b_{bw}(\lambda_2)+b_c^*(\lambda_2)C+b_p^*(\lambda_2)P]}{[a_w(\lambda_2)+a_c^*(\lambda_2)C+a_p^*(\lambda_2)P+a_y^*(\lambda_2)Y]} \tag{5}$$

$$R_{rs}(\lambda_3) = R_3 = \frac{c}{Q}\frac{[0.5b_{bw}(\lambda_3)+b_c^*(\lambda_3)C+b_p^*(\lambda_3)P]}{[a_w(\lambda_3)+a_c^*(\lambda_3)C+a_p^*(\lambda_3)P+a_y^*(\lambda_3)Y]} \tag{6}$$

where $b_{bw}(\lambda)$ = water backscattering coefficient

$b_p^*(\lambda)$ = sediment specific backscattering coefficient

$b_c^*(\lambda)$ = chlorophyll specific backscattering coefficient

$a_c^*(\lambda)$ = chlorophyll specific absorption coefficient

$a_w(\lambda)$ = pure water absorption coefficient

$a_y^*(\lambda)$ = yellow substance specific absorption coefficient

$a_p^*(\lambda)$ = sediment specific absorption coefficient.

Moreover, $b_{b(w)}(\lambda)$ is the water backscattering coefficient, and $b_{b(p)}^*(\lambda)$ and $b_{b(c)}^*(\lambda)$ are specific backscattering coefficients of sediment and chlorophyll, respectively. $a_c^*(\lambda)$ is the chlorophyll-specific absorption coefficient, $a_p^*(\lambda)$ is the sediment-specific absorption coefficient, and $a_w(\lambda)$ is the pure water absorption coefficient,. P, C, and Y are suspended particles, the concentrations of chlorophyll, and yellow substance, respectively (Gallie & Murtha, 1992).

3.4 Regression algorithm

TSS concentration can be calculated by solving the three simultaneous equations (4), (5) and (6) to obtain the series of terms R_1, R_2 and R_3 that is written as:

$$P = e_0 + e_1R_1 + e_2R_2 + e_3R_3 + e_4R_1R_2 + e_5R_1R_3 + e_6R_2R_3 + e_7R_1^2 + e_8R_2^2 + e_9R_3^2 \quad (7)$$

where the coefficients ej (j= 0,1,2, …,) are the functions related to the coefficients used in Equations (4) to (6), which are determined empirically from the multiple regression analysis. This equation is implemented to link reflectance values from the image bands to the observed TSS concentrations.

3.5 Image Processing

Raw images are corrected for distortions or degradations, due to the image acquisition process, by using a basic image processing technique. Radiometric and geometric corrections, masking and filtering are main components in the image processing (Albizua et al., 2012). In this study, PCI Geomatica digital image processing software (version 10.3) is used to carry out all image-processing tasks. The procedure shown in figure 4 is employed to extract reflectances from the raw ALOS image.

3.5.1 Geometric correction

To correct the raw ALOS image, image-to-image rectification was applied. Ground control points (GCPs) were determined by using a geometrically corrected (Système Pour l'Observation de la Terre (SPOT) satellite map as the reference geocoded image with root mean square error (RMSE) of less than 0.5 pixels (Kabbara et al. 2008). The primary steps used were as follows: recording of ground control points (GCPs), computing the transformation matrix, and resampling of the image. We chose and recorded 25 GCPs acquired from various geometrical locations such as ground level sharp corners, road junctions, and so on. If GCPs were conveniently identifiable in both the raw image and the reference, they are selected.

Next, the transformation matrix, which involves the coefficients for transforming the reference coordinate system to the input coordinate system, is used. Image rectification was conducted via first-order polynomial transformation equations to obtain an acceptable root mean square error (RMSE). Ultimately, the image was re-sampled to measure the values for the rectified image. The nearest neighbor re-sampling was implemented since this approach utilizes only the original brightness of the pixels.

Sample locations were then identified on these geocoded images. The RMSE, acquired for geometric correction of the images, was less than 0.5 pixels, which confirmed the high accuracy of the geometric correction (Kabbara et al., 2008).

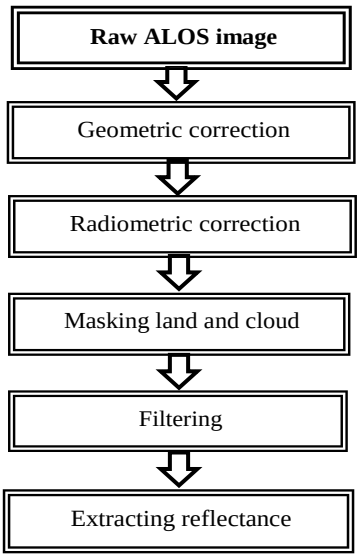

Fig. 4. Satellite imagery processing workflow.

3.5.2 Radiometric correction and extraction of reflectance data from ALOS images

Radiometric correction is concerned with eliminating the errors related to sensor detectors. Two major radiometric effects on satellite data were revealed by Ahern et al. (1987): earth-sun distance correction and sun elevation correction. The earth-sun distance correction is conducted to normalize the distance between the earth and the sun during seasonal changes. The sun elevation correction accounts for the seasonal position of the sun relative to the earth and it is implemented based on the angle of the sun from the zenith. Therefore, this correction compensates for different sun angles at different acquisition dates. After masking cloud and land, the digital numbers (DN) or pixel values of each band at the sample stations, were extracted using PCI software with a window size of 3x3 median filter (Kloiber et al., 2002). Applying median filter reduces the noise from a single pixel, hence, makes the output image smoother (Kabbara et al., 2008; Ma & Dai, 2005). In converting DN to reflectance, raw DNs were converted to radiance and then to reflectance. Radiance is linearly related to DN (Nanni & Dematte, 2006; Schroeder et al., 2006). First, the extracted DN values were converted into radiance values by:

$$L_\lambda = a * DN + b \tag{8}$$

where a is the spectral band gain, L_λ is spectral radiance at the sensor's aperture in ($Wm^{-2}sr^{-1}\mu m^{-1}$), and b is the spectral band offset (bais). The gain and offset values are unique for each spectral band acquired by a particular sensor. Then, the signal in each band and at each pixel was converted to At-Sensor Spectral Reflectance values using the following equation:

$$R_\lambda = \frac{\pi L_\lambda d^2}{E\,sun_\lambda \cos(\theta)} \tag{9}$$

where: d = Earth–Sun distance in astronomical units (AU)
R_λ= Unit less planetary reflectance
$E\,sun_\lambda$ = Mean solar exo-atmospheric irradiance ($Wm^{-2}\mu m^{-1}$)
θ = Solar zenith angle or (90- Sun Angle elevation) (°)

Gains and biases used for the conversion of digital numbers to spectral radiance for ALOS AVNIR-2 are presented in table 3. Earth-sun distance and sun angle elevation on 13 January 2008 and 18 January 2010 are demonstrated in table 4.

Table 3. Gains and biases used for the conversion of digital numbers to spectral radiance for ALOS AVNIR-2.

BAND	Physical gain	Bias	E sunλ ($Wm^{-2}\mu m^{-1}$)
1 (Blue)	0.5880	0	1943.3
2 (Green)	0.5730	0	1813.7
3 (Red)	0.5020	0	1562.3

Table 4. Earth- sun distance and sun angle elevation.

Date	Earth-Sun distance (AU)	Sun Angle Elevation (degree)
13.01.2008	0.98354	53.37
18.01.2010	0.98385	54.26

The reflectance values for all of the data points in three visible bands (blue, green, and red) were collected. Plots of suspended sediment concentrations versus the reflectance of the three visible bands were generated (Figure 5). As the TSS concentration increased, the response from each band also increased. Data points from the red band (band 3) were lower than those from the green band (band 2) and the blue band (band 1), both of which had shorter wavelength bands. These correlations indicate the effective relationship between the dependent variable, TSS, and the independent variables, reflectance of the bands.

4. Data analysis and results

4.1 Regression model development

Statistical methods are the most commonly applied techniques in calculating correlations between TSS concentration and spectral data (Asadpour et al., 2012; Y. Zhou et al., 2004). A linear regression analysis was implemented to test the relationship between ALOS bands and TSS concentrations of the entire database using the combined data from both image dates for multi-date analysis. The extracted reflectance for three visible bands was regressed with their respective sea-truth data using the SPSS 19 statistical analysis. A series of statistical models were developed and examined for specifying the best relation between measurements of TSS and reflectance of ALOS bands. Simple regression models between TSS and reflectance of individual bands (R_1, R_2, R_3) were investigated. The regression results

were evaluated based on statistical parameters such as determination coefficients (R^2) and root mean square error (RMSE) between the predicted and the measured TSS values and were utilized to demonstrate the importance of the regression model.

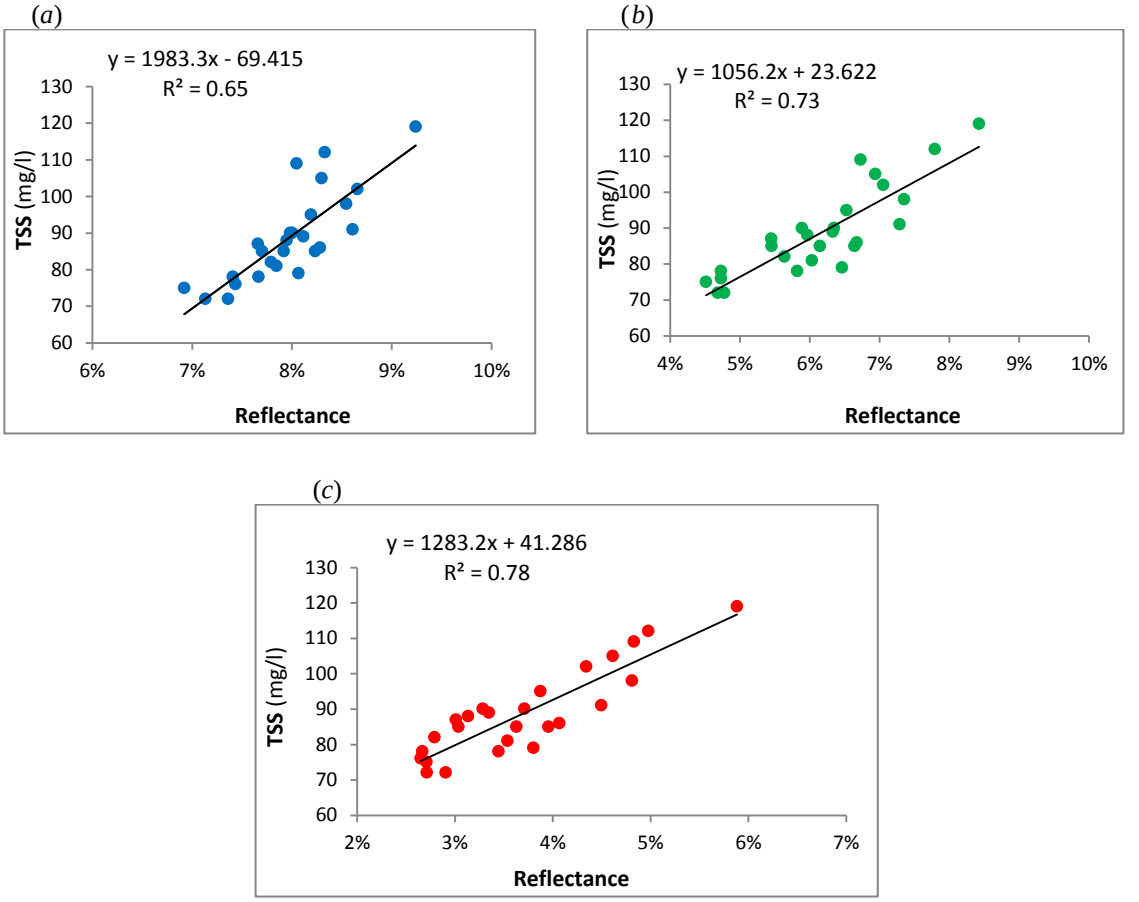

Fig. 5. TSS concentration (mg/l) versus reflectance of individual visible bands for (a) the blue band, (b) the green band and (c) the red band.

$$TSS = 1983.3(R_1) - \quad R^2 = \quad RMSE \approx 7.1 \tag{10}$$

$$TSS = 1056.2(R_2) + \quad R^2 = \quad RMSE \approx 6.2 \tag{11}$$

$$TSS = 1283.2(R_3) + \quad R^2 = \quad RMSE \approx 5.7 \tag{12}$$

where R_1, R_2 and R_3 express reflectance of band1 (blue), band2 (green) and band3 (red), respectively, and TSS is total suspended sediment in mg/l.

Furthermore, the multiple regression analysis was employed to calculate the relationship between the ALOS imagery data and TSS. The multiple regression analysis was conducted using reflectance combinations of the three visible ALOS bands (R_1, R_2, and R_3). The selection of the best regression equation for measuring TSS is made by comparing the correlation coefficients among these model equations. The best model should have highest R^2 and lowest RMSE to predict TSS from satellite imagery data. The weakest correlation was found in the simple regression models between reflectance of

single bands and TSS with ranged from 0.65 to 0.78, whereas the strongest correlation was obtained in a multiple regression model between reflectance combinations of the three visible bands and TSS with R^2 = 0.91. Thus a multiple regression model was selected to represent the best relation between the in-situ TSS and their corresponding reflectance values of ALOS bands. The highest correlation was reached in the non-linear relationship between the in-situ TSS and reflectance values of the bands. This trend coincides with the expression proposed by our algorithm in Equation (7). The derived algorithm generated a high correlation coefficient (R^2 = 0.91) and a low RMSE value (RMSE ≈ 3.52 mg/l) between the predicted and the measured TSS values. Subsequently, the TSS algorithm was applied to produce water quality maps of the study area. The proposed algorithm was achieved for the study area is:

$$TSS = -96677.9\ (R_1) +20329.17\ (R_2) +41093.55\ (R_3) +900667\ (R_1)^2 -361734\ (R_2)^2 -106222\ (R_3)^2 - 95604.5\ (R_1\ R_2) -1065221\ (R_1\ R_3) +848150.2\ (R_2\ R_3) +2492.743$$
$$(R^2 = 0.91 \quad RMSE \approx 3.52\ mg/l) \tag{13}$$

where R_1, R_2 and R_3 are reflectance of band 1 (blue), band 2 (green) and band 3 (red), respectively. This multi-date regression model includes reflectance of bands, interaction of bands reflectance and bands reflectance square with a high correlation coefficient and less root mean square error. Hence, we can conclude that this developed algorithm is satisfactory and can be successfully used to predict TSS concentrations. The predicted TSS values were computed via the proposed algorithm and were then correlated with their corresponding sea data measurements (Figure 6). As illustrated in figure 6, the data points are distributed relatively close to the straight line, that is, y ≈ x. Therefore, the non-linear algorithm provides efficient agreements between in-situ TSS concentration and predicted TSS.

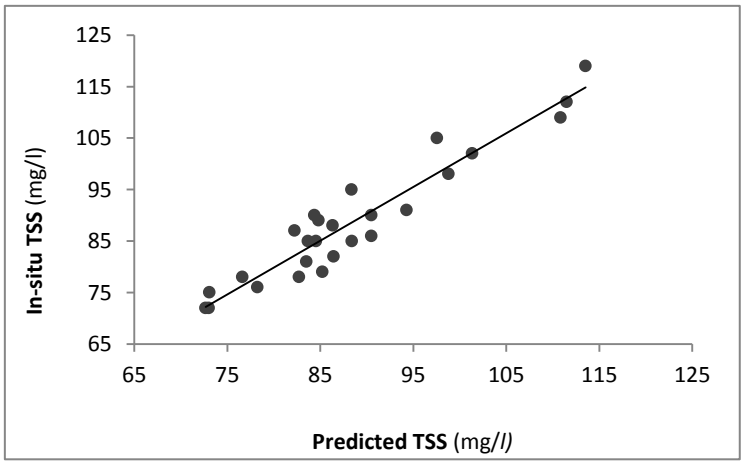

Fig. 6. In-situ TSS data versus predicted TSS data using combined data points.

4.2 Generation of TSS Map

The TSS concentration maps, which were estimated by applying the developed equations on the entire water surface of the Langkawi Island coastal waters based on the ALOS satellite images, were acquired. The suggested algorithms in Equation (13) created accurate results with R^2 =0.91 and RMSE ≈ 3.52 mg/l. The algorithm was applied to produce color-coded maps to define the range of pollution in the area. The maps were used for visual interpretation. The generated maps were filtered at 3 x 3 pixels that were

averaged to eliminate random noise. Figure 7 displays the TSS concentration maps of the coastal waters of Langkawi Island on 13 January 2008 and 18 January 2010.

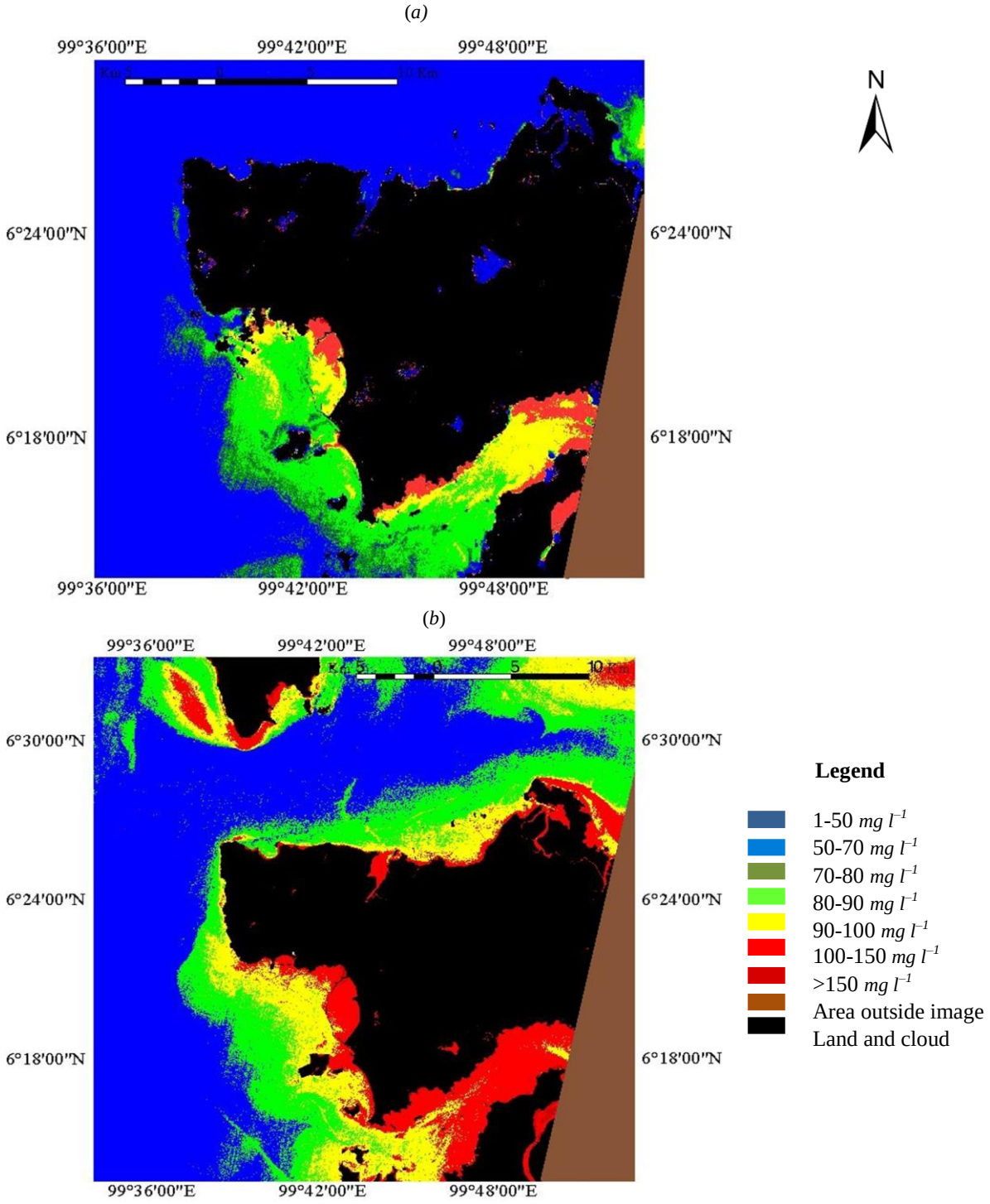

Fig. 7. TSS concentrations map created by using the new algorithm in the coastal waters of Langkawi Island on (a) 13 January 2008 (b) 18 January 2010.

5. Discussion

This study successfully used an efficient and cost-effective method in obtaining remote sensing data from the ALOS for remote sensing analysis. The approach and algorithm proposed in this study can resolve the challenges related to the conventional measurement of water quality. Besides, the application of the developed algorithm, by using the present data set, for mapping of TSS generated reliable and precise result. Therefore, the proposed algorithm was found to be a beneficial technique for water quality mapping of coastal water areas.

In this research, the best-fit regression equation for TSS prediction was identified through the regression approach. The regression model proved that the equation can be feasibly employed to measure the TSS concentrations of the coastal waters of Langkawi Island despite the unavailability of in-situ data. The result also revealed that as TSS concentration grows, the response from each ALOS band also boosts. Similar characteristics were reported by other researchers who utilized remote sensing invisible channels for suspended sediment studies (Alashloo et al., 2013; Asadpour et al., 2012; H. Lim et al., 2010; Syahreza, San, et al., 2011). These correlations indicated the positive relationship between independent variables (reflectance of bands) and dependent variables (TSS).

Comparison of the outcomes with other tested models shows that the extracted algorithm delivers the best predictive relationship. The highest correlation was obtained in the non-linear relationship between reflectance combinations of the three visible bands and in-situ TSS. Lim et al. (2008) and Schiebe et al. (1992) presented that the relationship between TSS and remote sensing data is not linear.

The algorithm can be effectively implemented in predicting TSS with $R^2 = 0.91$ and RMSE ≈ 3.52 mg/l when using satellite data. The derived algorithms in Equation (13) led to accurate results and were utilized to produce color-coded maps for visual interpretation. Several interesting patterns in the maps could be observed (Figure 7). Useful spatial information on water quality distribution patterns of coastal waters within the study area can be achieved from this kind of maps. This information is vital for coastal zone management and environmental planning. The data can be employed to determine the locations of erosion and deposition areas and to provide key information for the management and environmental planning of the marine environment.

The predicted TSS maps demonstrated higher concentrations of TSS in shallow water areas closer to the shoreline and the estuary of rivers. These areas are generally coastal environments with concentration values ranging from 100 mg/l to 150 mg/l or higher (red color). The highest water quality was observed in the deep clear water (shown in blue). Thus reflectance from TSS is more important in shorelines than that from signals coming from water far from the shore. As seen from the maps, the majority of the high values of TSS were concentrated in the southern part of the coastal waters of Langkawi Island because of urbanization. This finding indicated that the south is suffering from a much severe water quality problem than the north. The resultant concentration maps indicate that the concentration of TSS on13 January 2008 is lower than the concentration of TSS on 18 January 2010.

6. Conclusions

This study revealed that ALOS satellite is a useful tool for water quality mapping in the coastal waters of Langkawi Island. The procedures were conducted by developing and implementing regression models to ALOS data for estimating TSS concentrations. In addition, this study proved that TSS mapping can be performed over the study area using remote sensing techniques. The results from the combined data of two ALOS images in different dates stated that the measured TSS firmly agreed with the in-situ data with high correlation coefficients and lower root mean square errors. In sum, the results indicated that ALOS imagery and regression analysis can be used efficiently in calculating TSS concentrations in the coastal waters of Langkawi Island, Malaysia.

Acknowledgements

The authors wish to thank postgraduate students of Geophysics Program, School of Physics (USM) for assistance in field data acquisition and data processing.

References

Abdullah, K., MatJafri, M., Din, Z., Mahamod, Y., & Rainis, R. (2002). Remote sensing of total suspended solids in coastal waters of Penang, Malaysia. *Asian Journal of Geoinformatics*, *2*(2), 53-58.

Ahern, F., Brown, R., Cihlar, J., Gauthier, R., Murphy, J., Neville, R., & Teillet, P. (1987). Review article radiometric correction of visible and infrared remote sensing data at the Canada Centre for Remote Sensing. *International Journal of Remote Sensing*, *8*(9), 1349-1376.

Alashloo, M. M., Lim, H.-S., Asadpour, R., & Safarpour, S. (2013). Total Suspended Sediments Mapping by Using ALOS Imagery Over the Coastal Waters of Langkawi Island, Malaysia. *Journal of the Indian Society of Remote Sensing*, 1-11. doi:10.1007/s12524-012-0253-0

Albizua, L., Donezar, U., & Ibáñez, J. C. (2012). Monitoring urban development consolidation for regional management on water supply using remote sensing techniques. *European Journal of Remote Sensing*, *45*, 283-292.

Asadpour, R., Lim, H., Alashloo, M. M., Shekafti, S., & Moussavi, S. (2011). *Application of THEOS imagery to study Chlorophyll-a at the Strait of Penang Island, Malaysia*. Paper presented at the 2nd International Conference on Environmental Engineering and Applications, Shanghai, China.

Asadpour, R., San, L. H., Alashloo, M. M., & Moussavi, S. Y. (2012). A statistical model for mapping spatial distribution of total suspended solid from THEOS satellite imagery over Penang Island, Malaysia. *Journal of Applied Sciences Research*, *8*(1), 271-276.

Bresciani, M., Vascellari, M., Giardino, C., & Matta, E. (2012). Remote sensing supports the definition of the water quality status of Lake Omodeo (Italy). *European Journal of Remote Sensing*, *45*, 349-360.

Bruzzone, L., & Melgani, F. (2005). Robust multiple estimator systems for the analysis of biophysical parameters from remotely sensed data. *Geoscience and Remote Sensing, IEEE Transactions on*, *43*(1), 159-174.

Doxaran, D., Froidefond, J. M., Lavender, S., & Castaing, P. (2002). Spectral signature of highly turbid waters: Application with SPOT data to quantify suspended particulate matter concentrations. *Remote Sensing of Environment*, *81*(1), 149-161.

Gallegos, C. L., & Correll, D. L. (1990). Modeling spectral diffuse attenuation, absorption, and scattering coefficients in a turbid estuary. *Limnology and oceanography*, *35*, 1486-1502.

Gallie, E., & Murtha, P. (1992). Specific absorption and backscattering spectra for suspended minerals and chlorophyll-a in Chilko Lake, British Columbia. *Remote Sensing of Environment*, *39*(2), 103-118.

Giardino, C., Brando, V. E., Dekker, A. G., Strömbeck, N., & Candiani, G. (2007). Assessment of water quality in Lake Garda (Italy) using Hyperion. *Remote Sensing of Environment*, *109*(2), 183-195.

Guan, X., Li, J., & Booty, W. G. (2011). Monitoring Lake Simcoe water clarity using Landsat-5 TM images. *Water resources management*, 1-19.

Hakvoort, H., de Haan, J., Jordans, R., Vos, R., Peters, S., & Rijkeboer, M. (2002). Towards airborne remote sensing of water quality in The Netherlands—validation and error analysis. *ISPRS Journal of Photogrammetry and Remote Sensing*, *57*(3), 171-183.

Hariyanto, T., Taufik, M., & Solihuddin, T. (2011). Evaluation of multitemporal satellite images to identify total suspended solid change in Madura Strait waters. *Journal of Basic and Applied Scientific Research*, *1*(7), 583-588.

Hellweger, F., Schlosser, P., Lall, U., & Weissel, J. (2004). Use of satellite imagery for water quality studies in New York Harbor. *Estuarine, Coastal and Shelf Science*, *61*(3), 437-448.

Jordao, C., Pereira, M., Bellato, C., Pereira, J., & Matos, A. (2002). Assessment of water systems for contaminants from domestic and industrial sewages. *Environmental monitoring and assessment*, *79*(1), 75-100.

Kabbara, N., Benkhelil, J., Awad, M., & Barale, V. (2008). Monitoring water quality in the coastal area of Tripoli (Lebanon) using high-resolution satellite data. *ISPRS Journal of Photogrammetry and Remote Sensing*, *63*(5), 488-495.

Kamaruzzaman, B. Y., Shuhada, N. T., Shahbuddin, S., JalaL, K. A. C., AL-barwan, I. M., & Goddard, J. S. (2010). Spatial distribution of organic carbon contents of Langkawi island coastal waters, Malaysia. *Oriental Journal of Chemistry*, *26*(3), 851-855.

Kloiber, S. M., Brezonik, P. L., Olmanson, L. G., & Bauer, M. E. (2002). A procedure for regional lake water clarity assessment using Landsat multispectral data. *Remote Sensing of Environment*, *82*(1), 38-47.

Kratzer, S., Brockmann, C., & Moore, G. (2008). Using MERIS full resolution data to monitor coastal waters--A case study from Himmerfjärden, a fjord-like bay in the northwestern Baltic Sea. *Remote Sensing of Environment*, *112*(5), 2284-2300.

Lim, H., Jafri, M. Z. M., Abdullah, K., & Bakar, M. N. A. (2010). Water quality mapping using digital camera images. *International Journal of Remote Sensing*, *31*(19), 5275-5295.

Lim, H., MatJafri, M., Abdullah, K., Alias, A., Rajab, J., & Saleh, N. M. (2008). *Algorithm for TSS Mapping using satellite data for Penang Island, Malaysia*. Paper presented at the Fifth International Conference on Computer Graphics, Imaging and Visualization, Penang, Malaysia.

Lim, H., MatJafri, M., Abdullah, K., & Asadpour, R. (2011). *TSS mapping using THEOS imagery over Penang Island, Malaysia*. Paper presented at the The First International Conference on Interdisciplinary Research and Development, Thailand.

Lim, H., MatJafri, M., Abdullah, K., & Wong, C. (2009). *Total suspended solids (TSS) mapping using ALOS imagery over Penang Island, Malaysia*. Paper presented at the Computer Graphics, Imaging and Visualization, 2009. CGIV '09. 6th International Conference . Tianjin.

Lim, H. S., MatJafri, M. Z., Abdullah, K., & Asadpour, R. (2013). A Two-Band Algorithm for Total Suspended Solid Concentration Mapping Using THEOS Data. *Journal of Coastal Research*, 624-630. doi:10.2112/jcoastres-d-11-00152.1

Long, C. M., & Pavelsky, T. M. (2013). Remote sensing of suspended sediment concentration and hydrologic connectivity in a complex wetland environment. *Remote Sensing of Environment, 129*, 197-209. doi:https://doi.org/10.1016/j.rse.2012.10.019

Ma, R., & Dai, J. (2005). Investigation of chlorophyll‐a and total suspended matter concentrations using Landsat ETM and field spectral measurement in Taihu Lake, China. *International Journal of Remote Sensing, 26*(13), 2779-2795.

Massi, L., Santini, C., Pieri, M., Nuccio, C., & Maselli, F. (2011). Use of MODIS imagery for the optical characterization of Western Mediterranean waters. *Italian Journal of Remote Sensing, 4*, 19-17.

Matarrese, R., Chiaradia, M. T., Tijani, K., Morea, A., & Carlucci, R. (2011). 'Chlorophyll a'multi-temporal analysis in coastal waters with MODIS data. *Italian Journal of Remote Sensing, 4*, 9-48.

Nagamani, P., Hussain, M., Choudhury, S., Panda, C., Sanghamitra, P., Kar, R., . . . Rao, K. (2012). Validation of Chlorophyll-a algorithms in the coastal waters of Bay of Bengal initial validation results from OCM-2. *Journal of the Indian Society of Remote Sensing*, 1-9.

Nanni, M. R. D., & Dematte, J. A. M. (2006). Spectral reflectance methodology in comparison to traditional soil analysis. *Soil Science Society of America Journal, 70*(2), 393-407.

Park, E., & Latrubesse, E. M. (2014). Modeling suspended sediment distribution patterns of the Amazon River using MODIS data. *Remote Sensing of Environment, 147*, 232-242. doi:10.1016/j.rse.2014.03.013

Randolph, K., Wilson, J., Tedesco, L., Li, L., Pascual, D., & Soyeux, E. (2008). Hyperspectral remote sensing of cyanobacteria in turbid productive water using optically active pigments, chlorophyll and phycocyanin. *Remote Sensing of Environment, 112*(11), 4009-4019.

Schiebe, F., Harrington Jr, J., & Ritchie, J. (1992). Remote sensing of suspended sediments: the Lake Chicot, Arkansas project. *International Journal of Remote Sensing, 13*(8), 1487-1509.

Schroeder, T. A., Cohen, W. B., Song, C., Canty, M. J., & Yang, Z. (2006). Radiometric correction of multi-temporal Landsat data for characterization of early successional forest patterns in western Oregon. *Remote Sensing of Environment, 103*(1), 16-26.

Shafique, N., Autrey, B. C., Fulk, F., Cormier, S. M., & Environmental, S. B. (2001). The selection of narrow wavebands for optimizing water quality monitoring on the Great Miami River, Ohio using hyperspectral remote sensor data. *Journal of Spatial Hydrology, 1*(1), 1-22.

Siddorn, J., Bowers, D., & Hoguane, A. (2001). Detecting the Zambezi River plume using observed optical properties. *Marine pollution bulletin, 42*(10), 942-950.

Strickland, J. (1972). A practical handbook of seawater analysis. *Ottawa, Canada: Fisheries Research Board of Canada, 167*, 310.

Syahreza, S., Jafri, M. Z. M., San, L. H., Chun, B. B., & Mustapha, M. R. (2011). *Remote sensing for mapping surface water quality in coastal area of Aceh, Indonesia: Sendimentation effects of the December 2004 tsunami*. Paper presented at the Space Science and Communication (IconSpace), Penang, Malaysia.

Syahreza, S., San, L. H., Jafri, M. Z. M., & Mustapha, M. R. (2011). *Monitoring surface water quality in coastal area of Penang*. Paper presented at the International Conference on Environment Science and Engineering, Bali Island, Indonesia.

Zawada, D. G., Hu, C., Clayton, T., Chen, Z., Brock, J. C., & Muller-Karger, F. E. (2007). Remote sensing of particle backscattering in Chesapeake Bay: A 6-year SeaWiFS retrospective view. *Estuarine, Coastal and Shelf Science, 73*(3-4), 792-806.

Zhou, W., Wang, S., Zhou, Y., & Trony, A. (2006). Mapping the concentrations of total suspended matter in Lake Taihu, China, using Landsat TM data. *International Journal of Remote Sensing, 27*(6), 1177-1191.

Zhou, Y., Zhou, W., Wang, S., & Zhang, P. (2004). Applications of remote sensing techniques to inland water quality monitoring. *Advances in water science, 15*(3), 312-317.